Supporting information for:

Site-Specific Doping of Mn^{2+} in a CdS-based Molecular Cluster

Fumitoshi Kato and Kevin R. Kittilstved*

Department of Chemistry, University of Massachusetts Amherst, 374 Lederle GRT, 710 North Pleasant Street, Amherst, Massachusetts 01003, United States

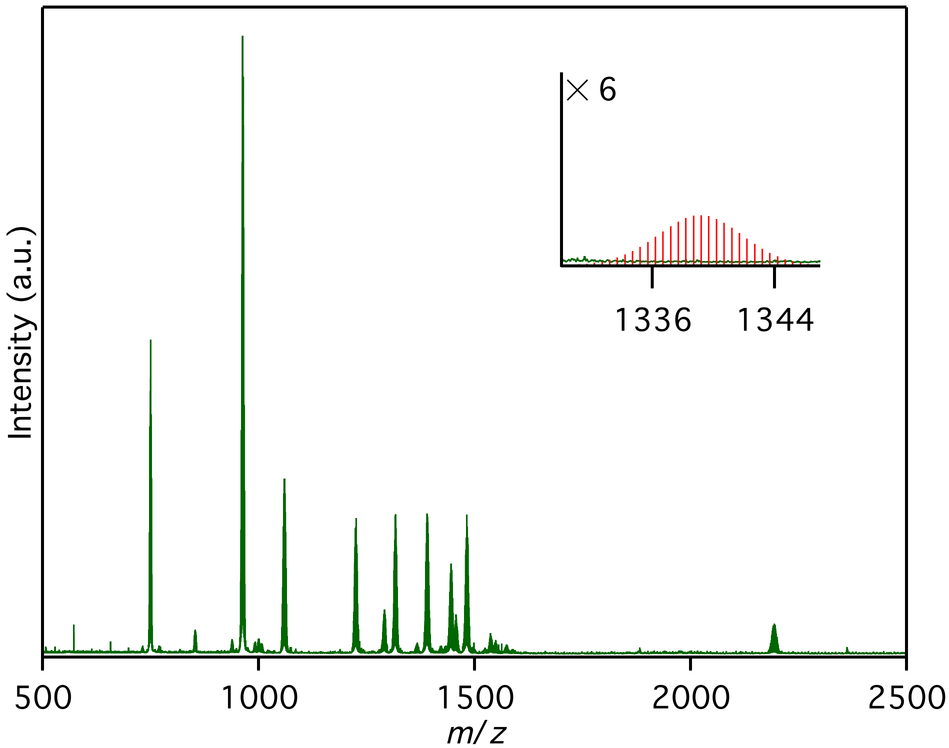

Figure S1. Negative ion mode ESI-MS of undoped Cd_{10} dissolved in CH_3CN collected at a cone voltage of −40V. The inset shows an overlay of the collected mass spectrum (green) and simulated $[Cd_8S(SPh)_{16}]^{2-}$ peak (red).

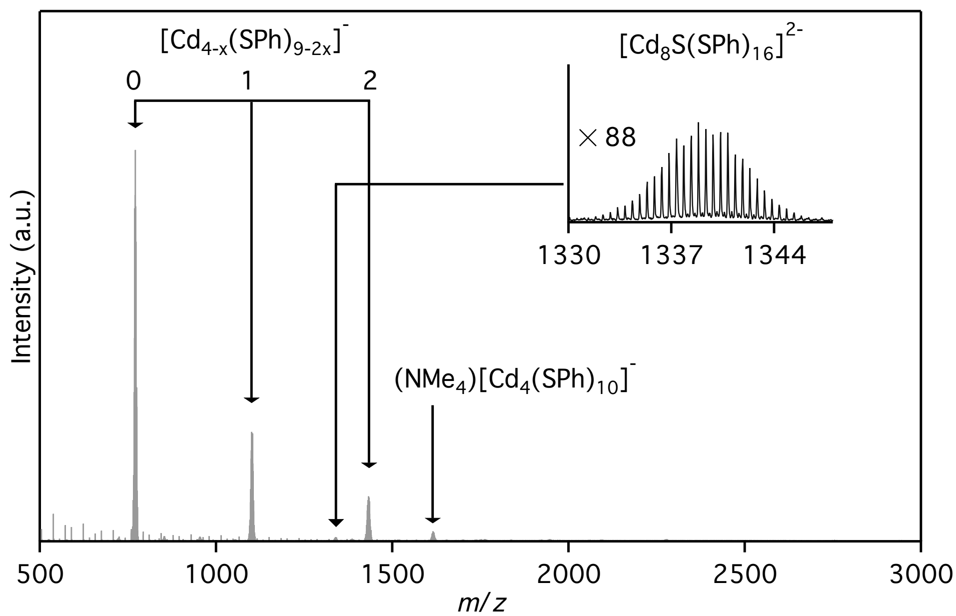

Figure S2. Negative-ion mode ESI-MS of the supernatant isolated after the synthesis of pure $\mathbf{Cd_{10}}$ was collected at a cone voltage of −40V. The dominant species detected by MS were the singly charged ions derived from $\mathbf{Cd_4}$. The numerical values shown in the graph corresponds to '*x*' in $[Cd_{4-x}(SPh)_{9-2x}]^{-}$. No peaks corresponding to fragments from $\mathbf{Cd_{10}}$ were observed.

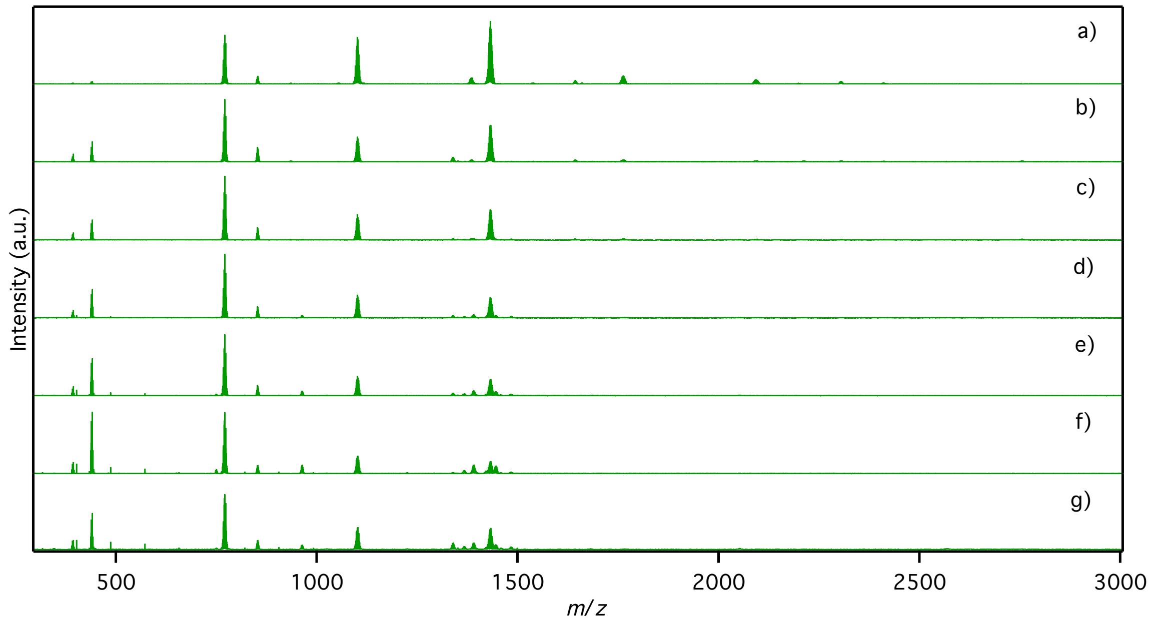

Figure S3. Negative-ion mode ESI-MS of the aliquots collected during the synthesis of undoped cluster. All the spectra were collected at a cone voltage of −20V. Mass spectra were collected after 2.14 mmol of $Cd(NO_3)_2$ (a), 240 µmol of Na_2S (b), 480 µmol of Na_2S (c), 720 µmol of Na_2S (d), 960 µmol of Na_2S (e), 1.20 mmol of Na_2S (f), and another 405 µmol of $Cd(NO_3)_2$ (g) was added a solution of 5.20 mmol of SPh^-.

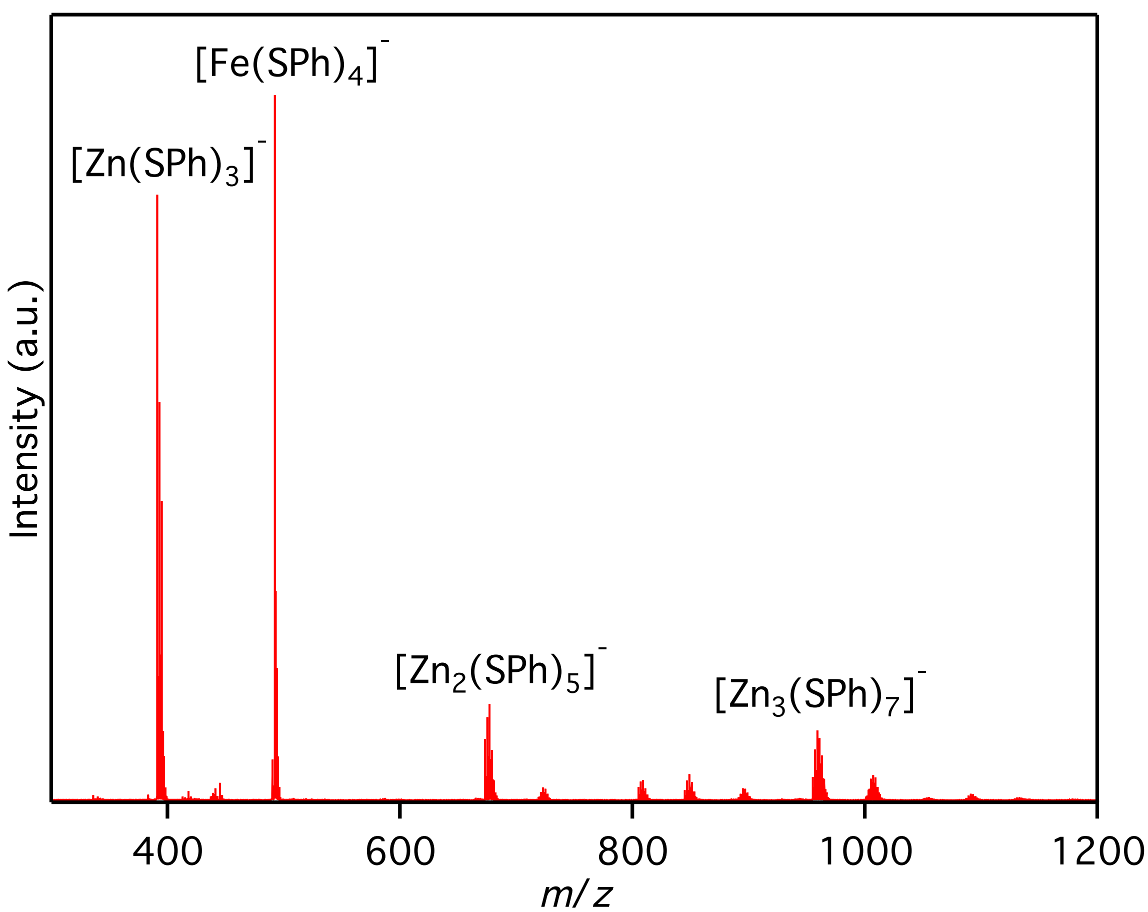

Figure S4. ESI-MS of thiophenol collected at −40V in CH_3CN. The ESI-MS exhibits a significant fraction of Zn^{2+} and Fe^{3+} contamination in the as-purchased bottle.

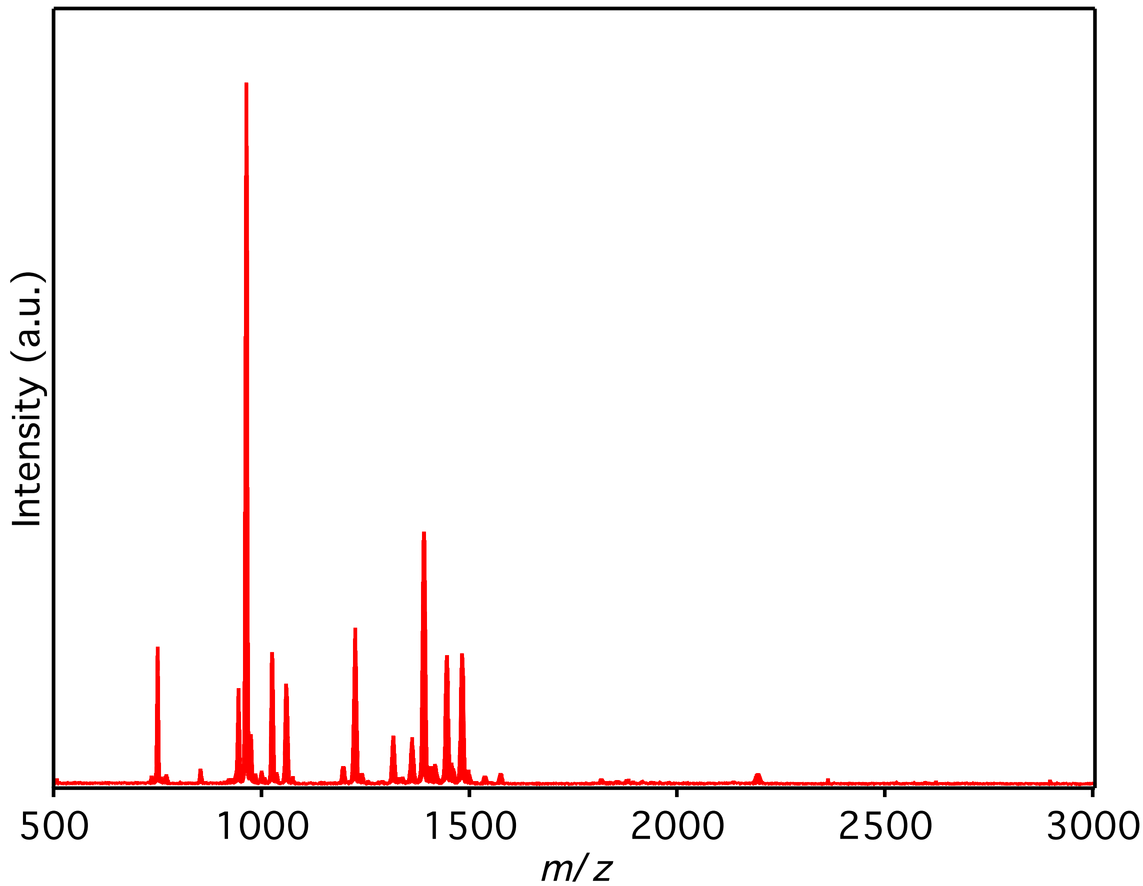

Figure S5. Mass spectrum of cluster prepared from **Mn:Cd$_{10}$-1**. The sample was dissolved in degassed acetonitrile and the spectrum was collected at a cone voltage of −40V.

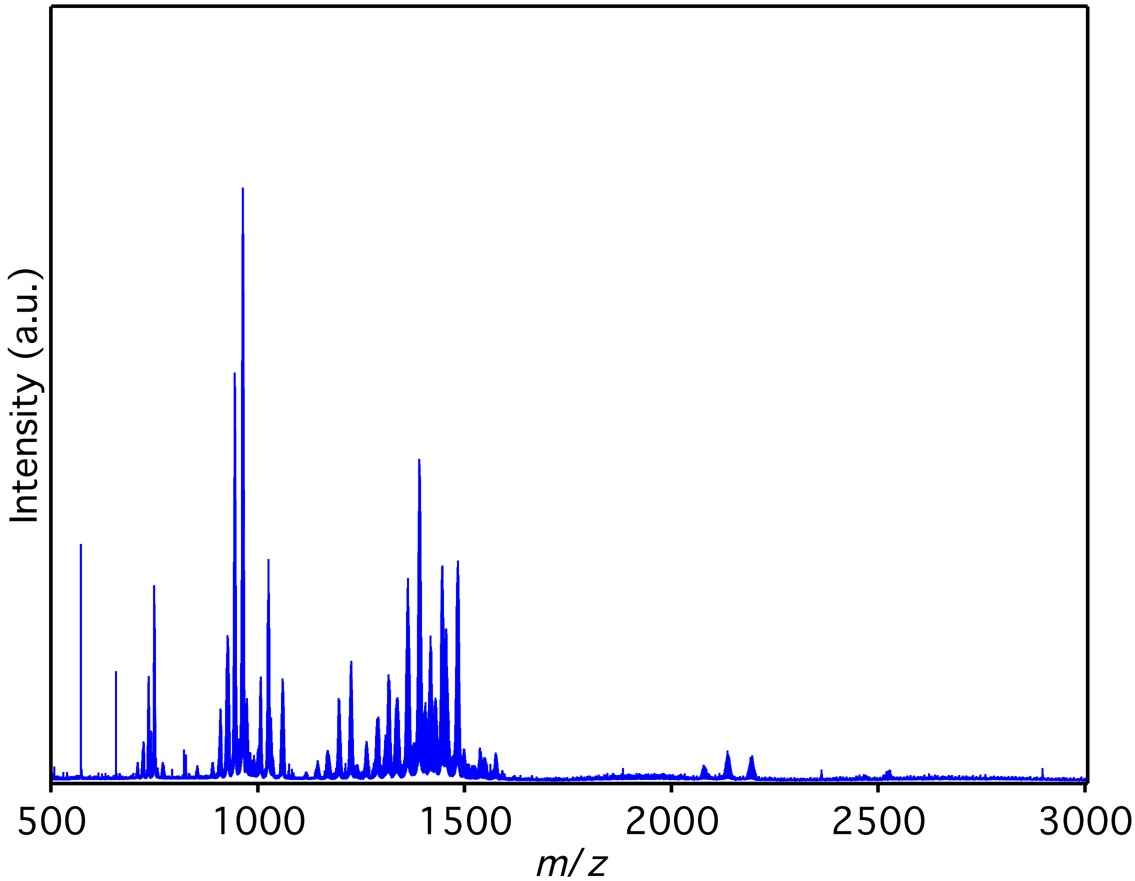

Figure S6. Mass spectrum of cluster prepared from **Mn:Cd$_{10}$-2**. The sample was dissolved in degassed acetonitrile and the spectrum was collected at a cone voltage of −40V.

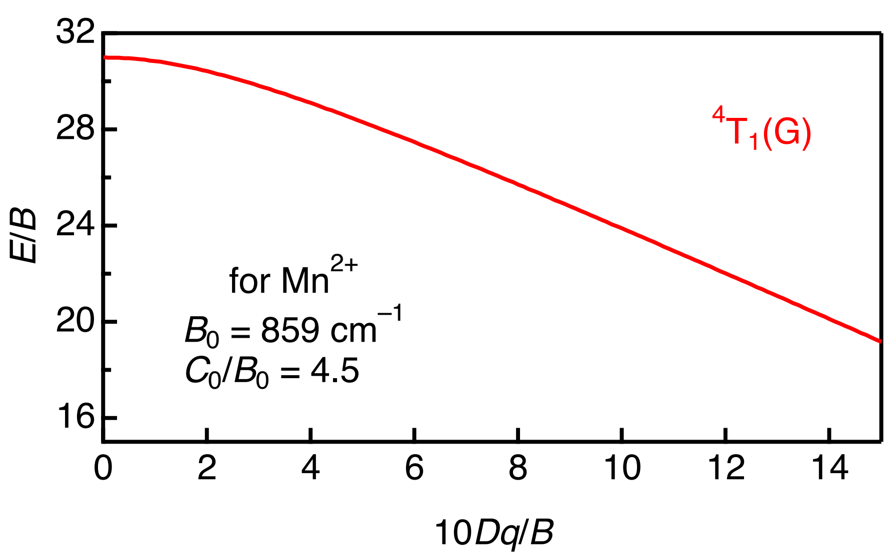

Figure S7. Expanded view of the lowest $^4T_1$ excited state energy (relative to the ground state) vs ligand field strength (10*Dq*/*B*) for a d^5 ion in a cubic field. The energies of the ground state and excited state was calculated using the Tanabe-Sugano energy matrices (see: Y. Tanabe, S. Sugano, On the Absorption Spectra of Complex Ions. I. *J. Phys. Soc.-Jpn* **1954**, *9*, 753-766).

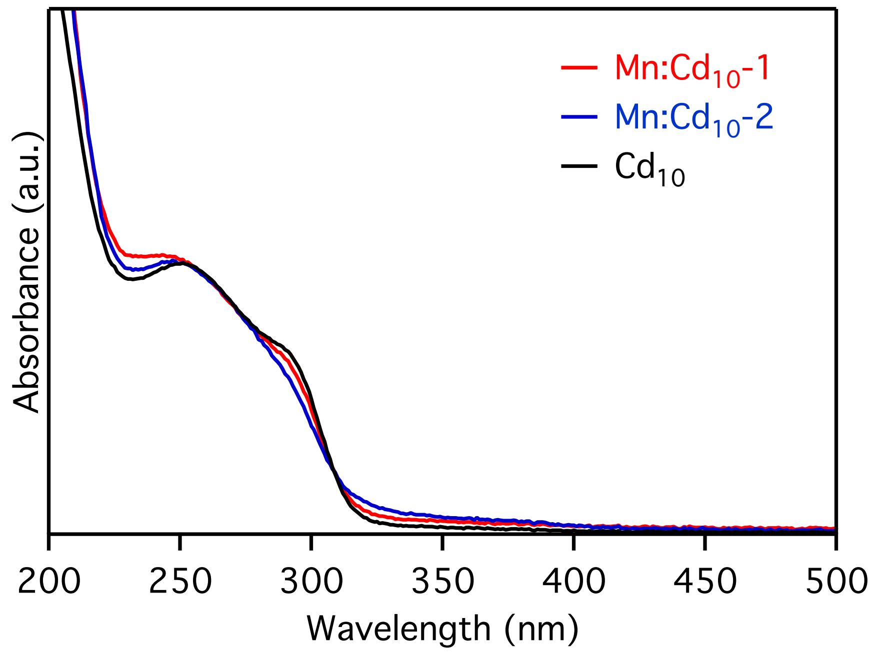

Figure S8. Room-temperature UV-Vis absorption spectra of the synthesized clusters dissolved in degassed acetonitrile.

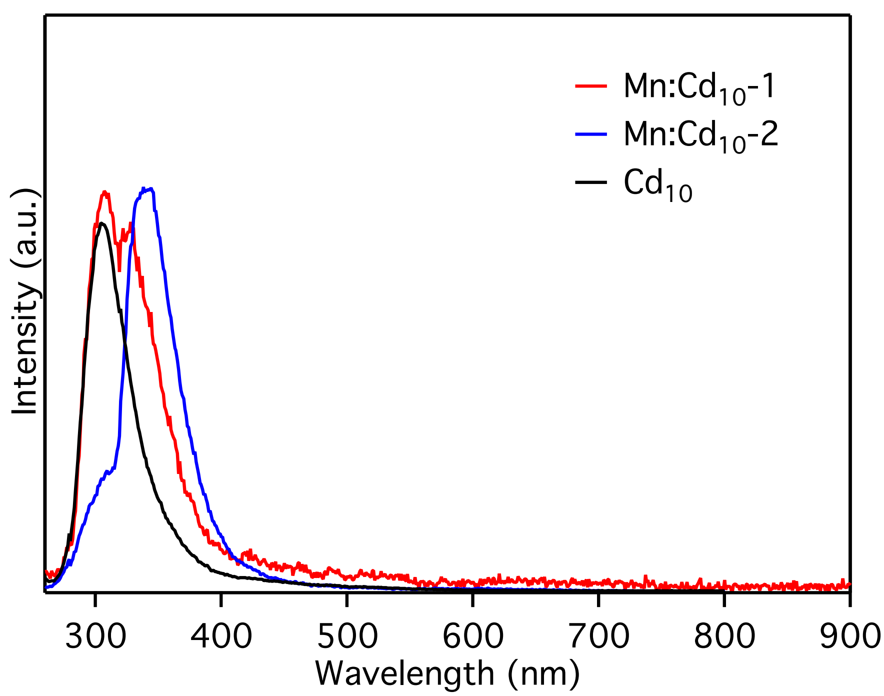

Figure S9. Room-temperature, steady-state PL spectra of the synthesized clusters dissolved in degassed acetonitrile. Samples were excited at 230 nm.

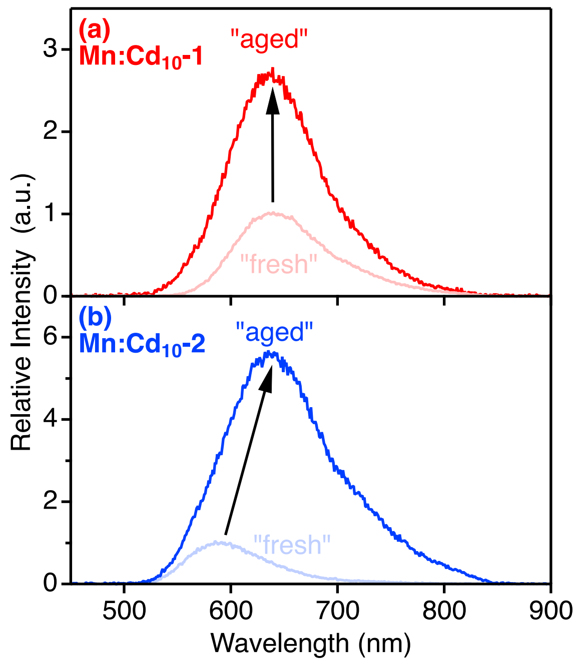

Figure S10. Room-temperature gated PL spectra of the **Mn:Cd$_{10}$-1** clusters collected immediately after the cluster was dissolved in degassed acetonitrile (red) and two hours later (yellow).

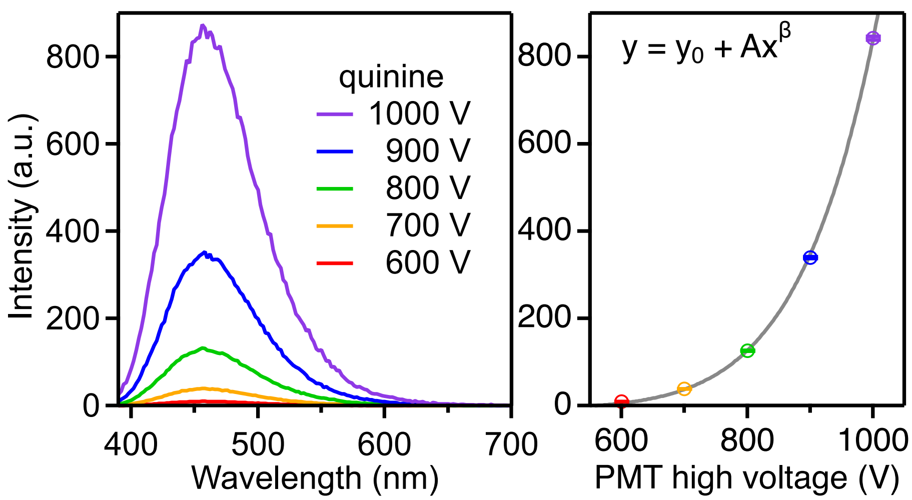

Figure S11. (Left panel) Steady-state PL spectra of a quinine sulfate dihydrate solution as a function of detector sensitivity (PMT high voltage). (Right panel) The intensity follows a power law dependence (gray line is the fit to the equation) ~6.7× enhancement in signal intensity upon increasing the PMT HV from 800 V to 1000 V. This scaling factor has been accounted for when normalizing the spectrum of the fresh Mn:Cd$_{10}$-2 shown in Figure 5 of the manuscript.

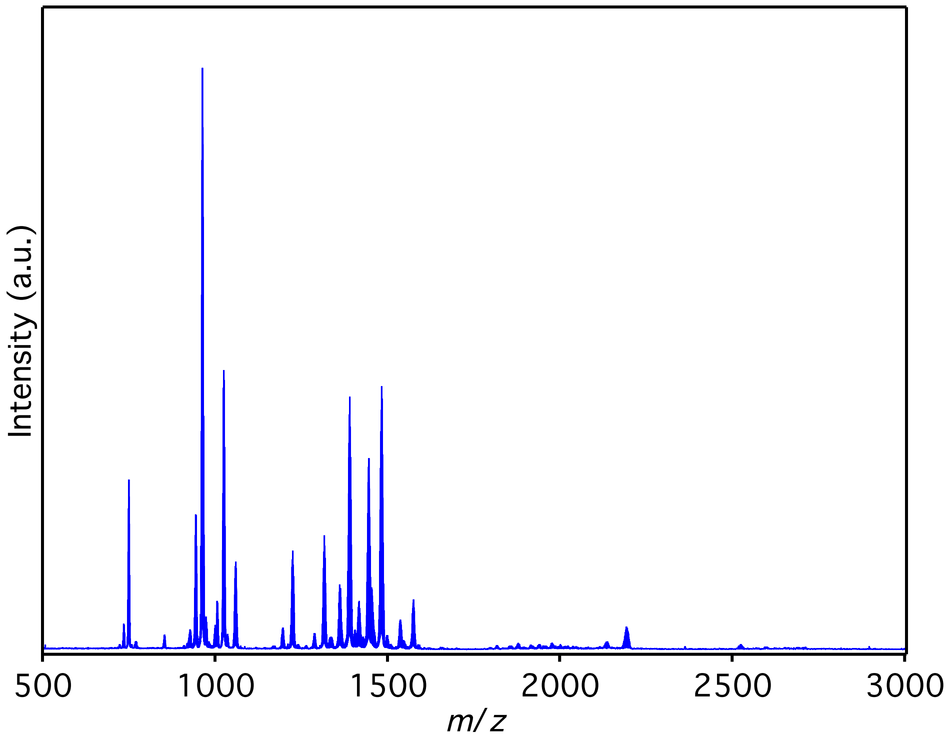

Figure S12. ESI mass spectrum of cluster prepared from **Mn:Cd$_{10}$-2**. The sample was dissolved in degassed acetonitrile for two hours before the spectrum was collected at a cone voltage of −40V.

Table S1. Anionic species observed in the mass spectra of clusters prepared by **Mn:Cd$_{10}$-1** or **Mn:Cd$_{10}$-2**. The cone voltage was set to −40V.

Fragments	*m*/*z* (calc.)	*m*/*z* (exp.)
$[NC_4H_{12}][Cd_8S_4(SPh)_{10}]^-$	2193	2193
$[NC_4H_{12}][Cd_7MnS_4(SPh)_{10}]^-$	2136	2136
$[NC_4H_{12}][Cd_6Mn_2S_4(SPh)_{10}]^-$	2078	2078
$[Cd_{10}S_3(SPh)_{16}]^{3-}$	1484	1484
$[Cd_9MnS_3(SPh)_{16}]^{3-}$	1455	1455
$[Cd_{10}S_4(SPh)_{15} + H^+]^{2-}$	1446	1446
$[Cd_9MnS_4(SPh)_{15} + H^+]^{2-}$	1417	1417
$[Cd_{10}S_4(SPh)_{14}]^{2-}$	1390	1390
$[Cd_9MnS_4(SPh)_{14}]^{2-}$	1362	1362
$[Cd_8Mn_2S_4(SPh)_{14}]^{2-}$	1333	1333
$[Cd_7Mn_3S_4(SPh)_{14}]^{2-}$	1304	1304
$[Cd_8S(SPh)_{16}]^{2-}$	1339	1339
$[Cd_7MnS(SPh)_{16}]^{2-}$	1310	1310
$[Cd_6Mn_2S(SPh)_{16}]^{2-}$	1282	1282
$[Cd_7S(SPh)_{14}]^{2-}$	1174	1174
$[Cd_6MnS(SPh)_{14}]^{2-}$	1145	1145
$[Cd_5Mn_2S(SPh)_{14}]^{2-}$	1117	1117
$[NC_4H_{12}][Cd_9S_4(SPh)_{13}]^{2-}$	1317	1317
$[NC_4H_{12}][Cd_8MnS_4(SPh)_{13}]^{2-}$	1288	1288
$[Cd_9S_4(SPh)_{12}]^{2-}$	1225	1225
$[Cd_8MnS_4(SPh)_{12}]^{2-}$	1196	1196
$[Cd_7Mn_2S_4(SPh)_{12}]^{2-}$	1168	1168
$[Cd_6Mn_3S_4(SPh)_{12}]^{2-}$	1139	1139
$[Cd_7S(SPh)_{14}]^{2-}$	1174	1174
$[Cd_6MnS(SPh)_{14}]^{2-}$	1145	1145
$[Cd_8S_4(SPh)_{10}]^{2-}$	1060	1060
$[Cd_7MnS(SPh)_{10}]^{2-}$	1031	1031
$[Cd_{10}S_3(SPh)_{17}]^{2-}$	1025	1025
$[Cd_9MnS_3(SPh)_{17}]^{2-}$	1006	1006
$[Cd_{10}S_4(SPh)_{15}]^{3-}$	963	963
$[Cd_9MnS_4(SPh)_{15}]^{3-}$	944	944
$[Cd_8Mn_2S_4(SPh)_{15}]^{3-}$	925	925
$[Cd_7Mn_3S_4(SPh)_{15}]^{3-}$	906	906
$[Cd_8S(SPh)_{17}]^{3-}$	929	929
$[Cd_7MnS(SPh)_{17}]^{3-}$	910	910
$[Cd_6Mn_2S(SPh)_{17}]^{3-}$	891	891
$[Cd_{10}S_4(SPh)_{16}]^{4-}$	750	750
$[Cd_9MnS_4(SPh)_{16}]^{4-}$	735	735
$[Cd_8Mn_2S_4(SPh)_{16}]^{4-}$	721	721
$[Cd_7Mn_3S_4(SPh)_{16}]^{4-}$	707	707
$[Cd_8S(SPh)_{18}]^{4-}$	724	724
$[Cd_7MnS(SPh)_{18}]^{4-}$	710	710
$[Cd_6Mn_2S(SPh)_{18}]^{4-}$	695	695

Table S2. Comparison of measured Mn and Zn contents for clusters prepared by method 1 and 2.

Elements	**Mn:Cd$_{10}$-1**	**Mn:Cd$_{10}$-2**
Mn	20.7%	20.1%
Zn	0%	0%

Table S3. Results from the double-exponential fit of the PL decay shown in Figure 4b using eq 1. Units are given next to the parameter.

Parameters	**Mn:Cd$_{10}$-1**	**Mn:Cd$_{10}$-2**
α_1 (a.u.)	0.090 ± 0.002	0.378 ± 0.045
τ_1 (ms)	0.120 ± 0.002	0.551 ± 0.039
α_2 (a.u.)	0.216 ± 0.002	1.169 ± 0.082
τ_2 (ms)	0.880 ± 0.016	3.141 ± 0.426
$\langle\tau\rangle$ (ms)	0.66	2.5